Complex Crude Oil Fouling Layers: Use of Model Predictions to Detect Inorganics Breakthrough

*Emilio Diaz-Bejarano (1), Francesco Coletti (1,2) and Sandro Macchietto (1,3)**

(1) Hexxcell Ltd., Innovation Hub, Imperial College - White City Campus, 80 Wood Lane, London W12 0BZ, UK

(2) College of Engineering, Design and Physical Sciences, Brunel University London, Uxbridge, UB8 3PH, UK

(3) Department of Chemical Engineering, Imperial College London, South Kensington Campus, London SW7 2AZ, UK

*E-main: s.macchietto@hexxcell.com

KEYWORDS: *crude oil, fouling, inorganics, heat exchanger, monitoring, diagnosis*.

ABSTRACT

Crude oil fouling models have greatly improved in the past two decades. However, most models focus on the deposition of organic species at high temperatures (i.e. greater than 200 °C). In this paper, a deposit model, capable of capturing simultaneously the deposition of both organic and inorganic species, is used to track deposition history in a shell-and-tube heat exchanger at the hot end of a refinery pre-heat train. The model was previously fitted to plant data and the results compared to the experimental characterization of deposits. It is shown that such a model, together with plant data, can be used i) to describe the development of complex deposit layers; ii) to detect and diagnose changes in composition of the deposit. From a practical perspective, it is then possible to alert plant operators of unexpected events such as breakthrough of inorganics at an early stage and help in planning corrective actions.

1. INTRODUCTION

Fouling in heat exchangers is a long-standing problem[1]. Most crude oil fouling models in the literature focus on the deposition of organic fouling species in heat exchangers, typically using functionality such as the Ebert-Panchal model[2] or its variants to describe the increase of fouling thermal resistance (R_f) over time. This family of models has been extensively reviewed and discussed in the past[3–7]. This may be a reasonable approximation when deposition is indeed of organic matter and caused by chemical reaction fouling, which typically occurs at high temperatures (i.e. greater than 200°C).

Recently, more descriptive models have emerged that view a deposit layer as a two-dimensional, dynamic multicomponent system, enabling capturing the effects of multiple species on an exchanger thermal and hydraulic performance as a function of process conditions and time[8]. This modelling approach has several advantages. First, the deposit growth is described in terms of mass fluxes, which determine the growth of the deposit thickness over time. The consequence is the calculation of the degree of blockage of the flow area and the immediate evaluation of the impact of fouling on pressure drops. The importance of considering the hydraulic impact of fouling has been highlighted in many past studies[9–13].

Second, the rate of deposition of the various species determines the local concentration through the deposit, which can be directly translated into local physical properties such as thermal conductivity. This property is essential to link the hydraulic impact of fouling to its thermal impact (i.e. on the rate of heat transfer), and hence obtain the overall effect that fouling has on the heat exchanger performance. The importance of identifying deposit thermal conductivity to assess the dominant impact of fouling (thermal or hydraulic) has been highlighted in the past, for example by Ishiyama *et al.*[11]. The thermal conductivity is ultimately function of the deposit nature and structure, and may vary over time if those change. Crude oil fouling deposits often contain significant proportions of inorganic materials, such as

carbonates, iron sulfides, and others[14–22]. These inorganics are characterized by higher conductivity than organic matter (1-5 W/m K vs. 0.2-1 W/m K, respectively), based on literature values[23–26]. Consequently, the presence of inorganic material should be accounted for in the deposit's conductivity to avoid errors in assessing the thermo-hydraulic performance of heat exchangers[27]. Diaz-Bejarano *et al.*[28] presented a simulation study for a s*ingle heat exchanger tube*, considering several types of inorganics in different proportions and using typical values for the deposition constants. The results showed that changes in fouling behavior result in complex layer structures, and suggested that understanding the impact of such dynamic behavior on the thermo-hydraulic performance of the exchanger is essential to develop efficient fouling monitoring and detection systems. To our knowledge, this was the first work that incorporated multiple fouling species, and particularly mixed inorganic and organic fouling, in the description of crude oil fouling deposits.

In this paper, the work by Diaz-Bejarano *et al.*[28] is extended to simulate the development of complex crude oil layer structures in a *complete shell-and-tube heat exchanger* at the hot end of a refinery pre-heat train. The exchanger model was previously fitted to plant data assuming mixed organic-inorganic deposition. A case study is presented here in which the heat exchanger undergoes chronic organic fouling and intermittent acute fouling episodes, resulting from inefficient desalter performance. First, the model is used to illustrate the formation of sub-layers of different composition and how these relate to deposit thickness build-up, conductivity and heat transfer. Then, the impact of such deposition history on the thermal and hydraulic performance of the exchanger is evaluated. Finally, it is discussed how these concepts could be used in practice to detect inorganic breakthrough based on online monitoring of measurable operating conditions.

2. MODEL DESCRIPTION

The fouling deposit is described by the multi-component, distributed deposit model by Diaz-Bejarano *et al.*[8]. The model has the ability to retain composition history at each point through the deposit and along the heat exchanger under all circumstances. The deposit model is used within Hexxcell Studio™, a software suite for the analysis, design and operations support of thermal systems undergoing fouling[29]. The modelling framework is schematically shown in Fig. 1. The main equations of the shell-and-tube heat exchanger model are summarized in Table 1 and Eq. 1 - 7 below.

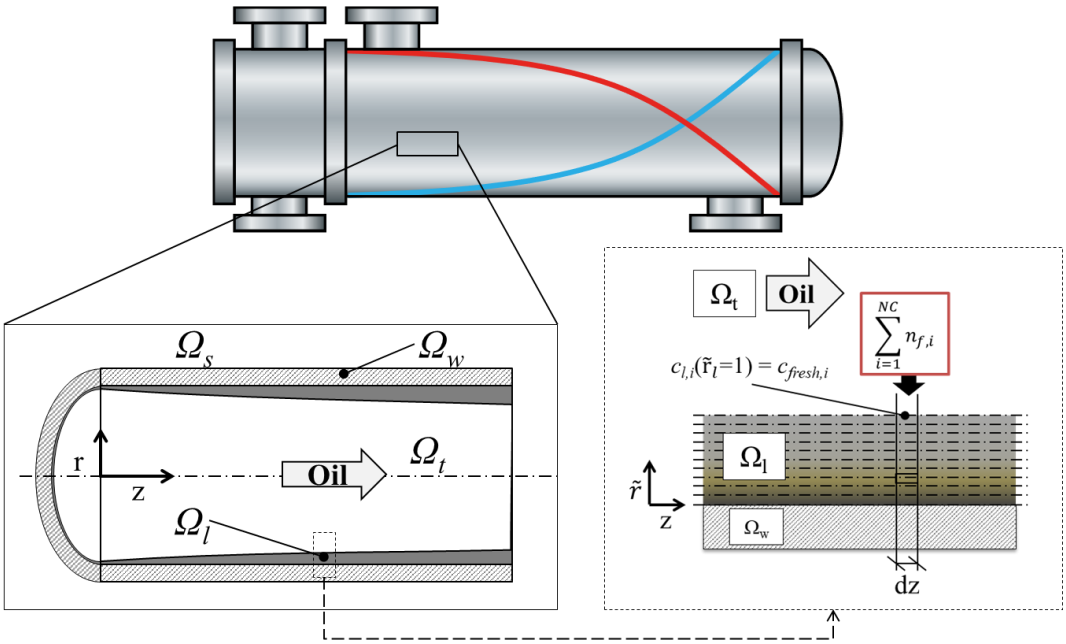

Fig. 1 Schematic representation of a growing fouling layer at a particular location along a heat exchanger tube within a shell-and-tube heat exchanger (adapted from Diaz-Bejarano *et al.*, 2016b).

Table 1. Main equations of the heat exchanger model by Coletti and Macchietto[30] (adapted from [31])

Tube-Side (Ω_t)	
Energy balance	$\frac{\partial\left(A_{t,n}(z)\rho_n(z)H_n(z)\right)}{\partial t} = -dir_n\frac{\partial\left(A_{t,n}(z)\rho_n(z)u_n(z)H_n(z)\right)}{\partial z} + p_n(z)h_n(z)(T_{l,n}\big\vert_{R_{flow,n}}(z) - T_n(z))$
	$h_n(z)$ calculated by Sieder-Tate correlation [32]
Pressure drop	$\Delta P_{total} = \Delta P_{External} + \Delta P_{Headers} + \sum_{n=1}^{N_p}\left(P_{n,in} - P_{n,out}\right)$
	$-\mathrm{dir}_n\frac{dP_n(z)}{dz} = \frac{C_f(z)\rho_n(z)u_n(z)^2}{R_{flow,n}(z)} = \frac{2\tau_{w,n}(z)}{R_{flow,n}(z)}$
	$C_f = f(Re_n)$ [33]
Shell-side (Ω_s)	
Energy balance	$\frac{\partial(A_s\rho_s(z)H_s(z))}{\partial t} = -dir_s\frac{\partial(A_s\rho_s(z)u_s(z)H_s(z))}{\partial z} + \sum_{n=1}^{N_p} p_{s,n}h_s(z)(T_s(z) - T_{w,n}\big\vert_{r=RO}(z))$
	$h_s(z)$ calculated with Bell-Delaware method [34]
Tube wall (Ω_w)	
Energy balance	$\rho_{w,n}C_{p,w,n}(z,r)\frac{\partial T_{w,n}(z,r)}{\partial t} = \frac{1}{r}\frac{\partial}{\partial r}\left(r\lambda_w\frac{\partial^2 T_{w,n}(z,r)}{\partial^2 r}\right)$

The main model equations of the deposit layer domain ($\boldsymbol{\Omega_l}$) are:

- Mass balance for component i (i = 1, … N) considering *NR* chemical reactions:

$$\left(\frac{\partial c_{l,i}(z,\tilde{r}_l)}{\partial t} - \frac{\tilde{r}_l}{\delta_l(z)}\dot{\delta}_l(z)\frac{\partial c_{l,i}(z,\tilde{r}_l)}{\partial \tilde{r}_l}\right) = \sum_{j=1}^{NR}\nu_{ij}r_j(z,\tilde{r}_l) \tag{1}$$

- Energy balance:

$$\rho_l(z,\tilde{r}_l)C_{p,l}(z,\tilde{r}_l)\left(\frac{\partial T_l(z,\tilde{r}_l)}{\partial t} - \frac{\tilde{r}_l}{\delta_l(z)}\dot{\delta}_l(z)\frac{\partial T_l(z,\tilde{r}_l)}{\partial \tilde{r}_l}\right) = \frac{1}{(R_i-\tilde{r}_l\delta_l(z))\delta_l(z)^2}\frac{\partial}{\partial \tilde{r}_l}\left((R_i - \tilde{r}_l\delta_l(z))\lambda_l(z,\tilde{r}_l)\frac{\partial T_l(z,\tilde{r}_l)}{\partial \tilde{r}_l}\right) \tag{2}$$

where $c_{l,i}$ is the mass concentration of component *i*, *t* time, $\tilde{r}$ the dimensionless radial coordinate, δ the deposit layer thickness, $\dot{\delta}$ the rate of change in thickness, r_j the rate of reaction *j*, R_i the inner tube radius, T_l temperature, *z* the axial coordinate, ρ_l density, $C_{p,l}$ specific heat capacity, v_{ij} stoichiometric coefficient for component *i* in reaction *j* and λ_l thermal conductivity of the mixture at each point $(z, \tilde{r})$. The conductivity of the deposit at each point, λ_l (z,r), is function of the local concentration of fouling species. Distinct thermal conductivity mixing models can be used to relate λ_l (z,r) to $c_{l,i}$(z,r), each representing different deposit material

structures. Here, a Co-continuous conductivity mixing model (originally introduced by Wang *et al.*[35] is used to calculate the local thermal conductivity of the deposit as a function of the local concentration of the organic and inorganic components at each point (z, r):

$$\lambda_l(z,\tilde{r}_l) = \frac{\sqrt{1+8\left(x_{l,org}\lambda_{org}+x_{l,inorg}\lambda_{inorg}\right)\left(x_{l,org}/\lambda_{org}+x_{l,inorg}/\lambda_{inorg}\right)}-1}{2\left(x_{l,org}/\lambda_{org}+x_{l,inorg}/\lambda_{inorg}\right)} \quad (3)$$

where x_l is the local volume fraction of the organic (*org*) or inorganic (*inorg*) component.

The change in deposit thickness depends on the net deposition rates of the various species. Here, a binary system comprising one organic and one inorganic pseudo-component is considered. The overall deposition rate is (*n*):

$$n(z) = n_{inorg}(z) + n_{org}(z) \quad (4)$$

The change in thickness of the deposit is:

$$\dot{\delta}_l(z) = \frac{n_{inorg}(z)}{\rho_{inorg}} + \frac{n_{org}(z)}{\rho_{org}} \quad (5)$$

The organic deposition is described by a typical crude oil fouling correlation. This deposition serves as baseline to describe the usual or expected fouling behavior. The functional form of the threshold model by Panchal *et al.*[36] is used to describe organic deposition as function of tube-side film temperature and shear stress:

$$n_{org}(z) = \alpha' Re_n(z)^{-0.66} Pr_n\,(z)^{-0.33}\, exp\left(\frac{-E_f}{RT_{film}(z)}\right) - \gamma'\tau_{w,n}(z) \quad (6)$$

Where n_{org} is the deposition rate of the organic component, *Re* the Reynolds number, *Pr* the Prandtl number, T_{film} the film temperature, τ_w the wall shear stress (at the surface of the deposit), *z* the axial coordinate, subscript *n* the pass number, and α', *Ef*, γ' are the three adjustable parameters. The physical properties in *Re* and *Pr* are functions of the local bulk temperature.

Following the approach introduced by Diaz-Bejarano *et al.* [28], the deposition of inorganics is regarded as a deviation from that baseline. It is described as a relative deposition rate with respect to the organic rate by means of a proportionality ratio p_{inorg}:

$$n_{f,inorg,n}(z) = p_{inorg} n_{f,org,n}(z) \rho_{inorg} / \rho_{org} \quad (7)$$

The proportionality ratio may be imposed (either fixed or time-varying) to simulate scenarios of interest. If sufficient information is available, it may also be estimated from experimental and measured data[31,37].

3. CASE STUDY

The case study considers a double-shell heat exchanger (called shell A and shell B) located after the desalter of a refinery pre-heat train. The geometry of the exchanger and physical properties of the fluids are provided in ref.[31]. The organic and inorganic phases are assumed to be characterized by thermal conductivity of 0.2 W/mK and 4 W/mK, respectively, as justified in that paper. The fouling species are assumed not to take part in any chemical reactions or other transformations once they are settled as part of the deposit layer (i.e. the term in the right-hand side of Eq. (1) is equal to zero). In this section, the model is used to simulate the build-up of a complex layer structure following malfunctioning of the desalter equipment over a period of 400 days. The mal-operation of desalters is often associated to temperature or throughput variations (for example, operation at over-capacity[21]) or occasional processing of feedstock containing large quantities of particles and/or inorganic species. Here, for simplicity, the inlet operating conditions to the heat exchanger (temperature, flowrate) are kept constant throughout the simulation. The heat exchanger is assumed to undergo slow chronic fouling dominated by organic deposition. The organic reference deposition rate is given by the previously discussed model, that was fitted to an extensive, four-year set of plant data[37]. A small fraction of inorganic

(p_{inorg} = 0.15) is also assumed to deposit together with the organic under normal circumstances. The key model parameters used in the case study are summarized in Table 2.

Table 2. Main parameters used in the case study[31,37]

Exchanger Geometry		**Fluids Properties**			**Fouling**	
Parameter	Value	Parameter	Tube-side fluid	Shell-side fluid	Parameter	Value
N_s	2	Fluid	Crude Oil	VGO	α' (kg_{org} $m^{-2}s^{-1}$)	0.70
Arrangement	Counter-current flow	API	33.88	23.36	$10^9\gamma'$ (kg_{org} $m^{-2}s^{-1}Pa^{-1}$)	1.23
Pass	2	MeABP (ºC)	221.3	412.3	E_f (kJ mol^{-1})	28.5
D_s (mm)	1194	$\nu_{38ºC}$ (cSt)	6	50	λ_{inorg} (W $m^{-1}K^{-1}$)	4
D_o (mm)	19.86	T_{in} (ºC)	140	280	λ_{org} (W $m^{-1}K^{-1}$)	0.2
D_i (mm)	25.4				ρ_{inorg} (kg m^{-3})	3200
N_t	844				ρ_{org} (kg m^{-3})	2360

A p_{inorg} time-history profile, shown in Fig. 2, is imposed to simulate periods of large inorganic breakthrough. This profile assumes that the desalter starts malfunctioning about 150 days after operation starts. Inorganics breakthrough is assumed to occur over three distinct periods (this could be due, for instance, to desalting malfunctioning under specific conditions or operations determined by external factors). Based on the observations in ref.[37], it is postulated that the intensity of the inorganic-to-organic deposition ratio during breakthrough periods decreases over time to reflect the impact of shear stress, increased by the presence of the deposit itself, on deposition.

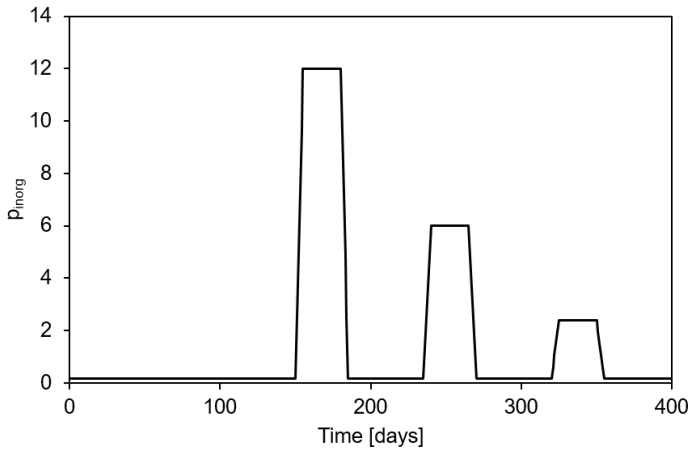

Fig. 2. Inorganic-to-organic proportionality ratio (p_{ionrg}) over the operation period considered.

3.1. Complex Layers Structures

The alternation of chronic organic-dominated fouling build-up and the acute inorganic deposition periods leads to the deposit growth in Fig. 3, as given by the average deposit thickness. The fouling build-up is initially moderate. After 150 days, coinciding with the first acute episode, there is a fast build-up of material. The thickness grows quickly from 0.65 to 1.65 mm during this period. After the acute episode finishes (day 180), the fouling behavior returns to the usual organic one. However, the fouling rate is slower now compared to the initial period (before day 150). The inorganic breakthrough episode leads to a substantial blocking of the available flow area, resulting in increased shear stress and lower net deposition rate. The second episode, starting after 230 days, also results in a fast fouling build-up, although to a lesser extent. Finally, the third episode is barely noticeable compared to the previous ones. At that stage, the chronic organic fouling is approaching a plateau as a result of the very high shear stress.

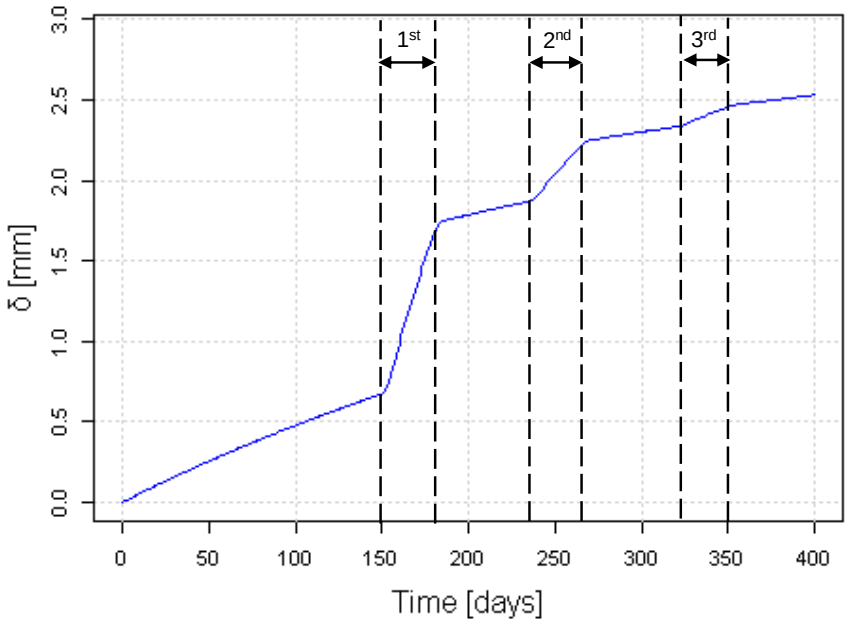

Fig. 3. Average deposit thickness over 400 days with intermittent inorganic breakthrough episodes. Vertical dashed lines and the labels in-between indicate the three high inorganic deposition periods.

The above schedule of events results in the formation of a stratified deposit, characterized by a composition radial profile evident from the deposition history (similar to a tree's growth rings). The resulting distribution of the deposit's properties in the radial direction are explained below for a particular exchanger location, the exit of the second pass of Shell B, indicated in the sketch in Fig. 4. This point is located at approximately the middle of the crude oil path through the double-shell exchanger and, therefore, is characterized by intermediate operating conditions between inlet an outlet.

The resulting composition radial profile at the end of the time period considered is shown in Fig. 5, where the inorganic content is plotted against the distance from the metal tube wall. The surface of the deposit is indicated by a vertical dashed line. The portion of the deposit next to the wall corresponds to the initial 150 days of operation, dominated by organic deposition. After that, the three acute fouling episodes are observed as three progressively smaller peaks in inorganic content. The first episode, of greater magnitude, is observed as a large deposit layer with high-inorganic content (>90$_{wt}$%) located between 0.65-1.65 mm from the wall.

The deposition rate, composition and structure of the deposit determine its thermal conductivity. The conductivity radial profile corresponding to the composition profile in Fig. 5, is shown in Fig. 6. The deposit is characterized by a $\lambda_l \approx 0.5$ W/mK for the layer up to the first 0.5 mm from the wall, where the deposit is mainly organic. After that, the conductivity increases as a result of the large amount of inorganics deposited during the first acute fouling episode, with a maximum $\lambda_l = 2.75$ W/mK. After that, sub-layers of high conductive and low conductive material alternate.

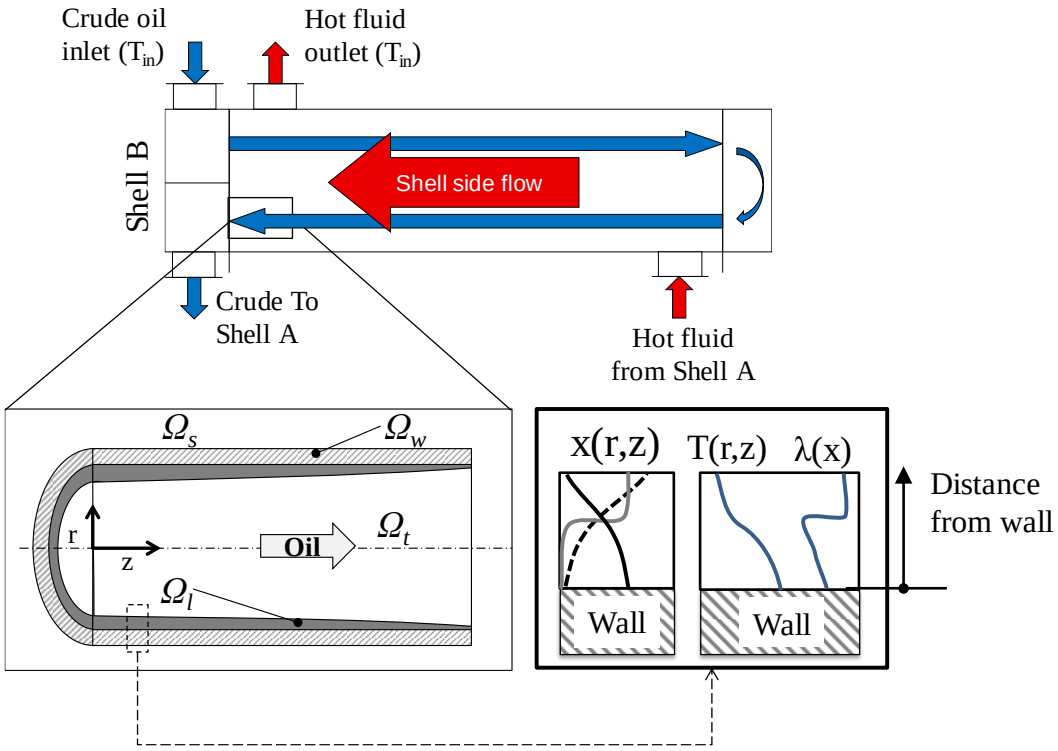

Fig. 4. Sketch indicating the radial location used to explain the radial distribution of the properties in the deposit in Figs. 5-7 (exit of the 2nd pass of shell B).

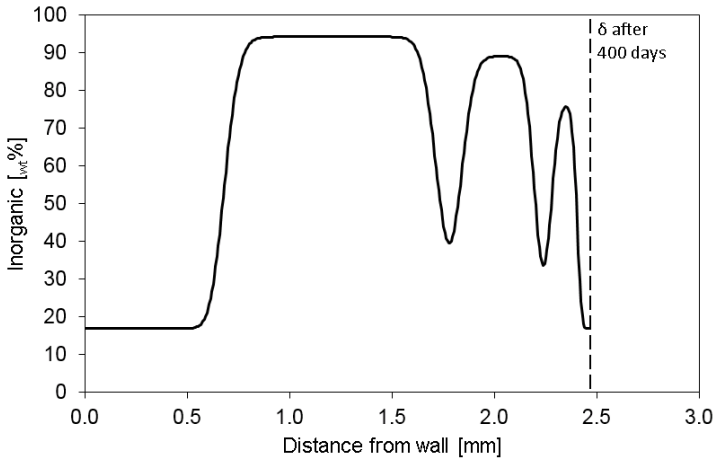

Fig. 5. Radial inorganic content profile in the deposit, at the exit of the 2nd pass of shell B, at the end of the operation period.

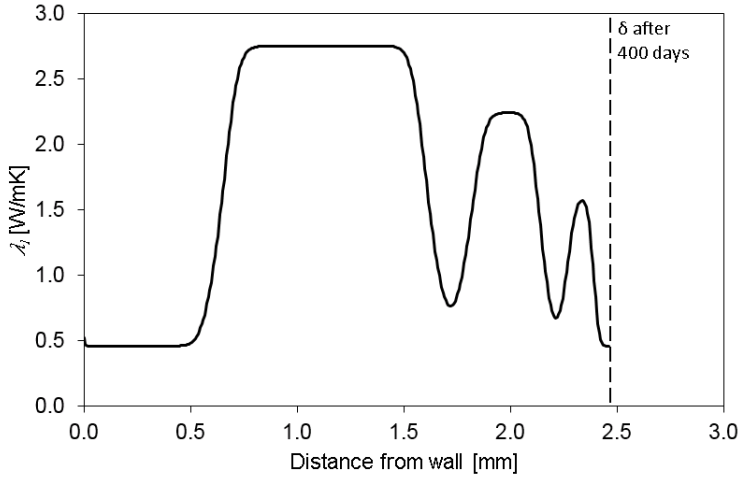

Fig. 6. Radial thermal conductivity profile in the deposit at the exit of the 2nd pass of shell B, at the end of the operation period.

The above compositional layered structure and resulting conductivity profile affect the rate of heat transfer between tube and shell-side fluids. This is reflected in the radial temperature profile at the fouling deposit, shown in Fig. 7 for the same location as Fig. 5 and Fig. 6. Fig. 7 shows several screenshots of temperature profiles at various times of interest. The vertical dashed lines indicate the deposit thickness surface at the time indicated with an adjacent text label. After 150 days (Fig. 7a, black line), the deposit has introduced a substantial resistance to heat transfer.

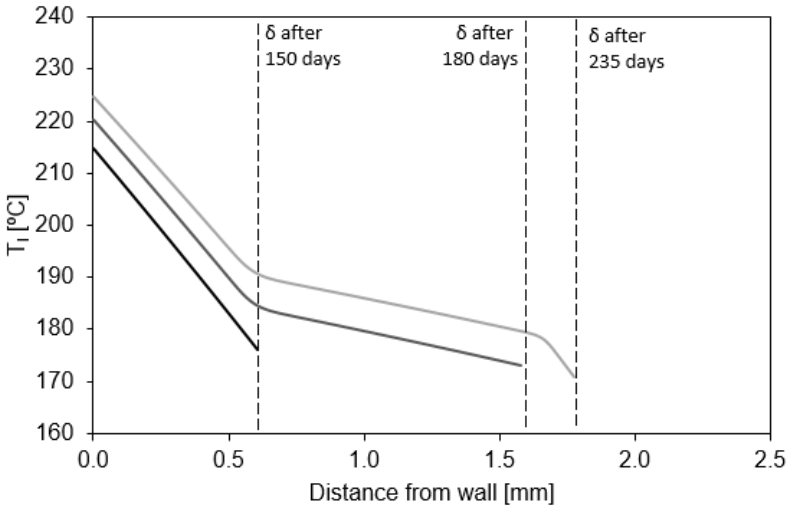

(a)

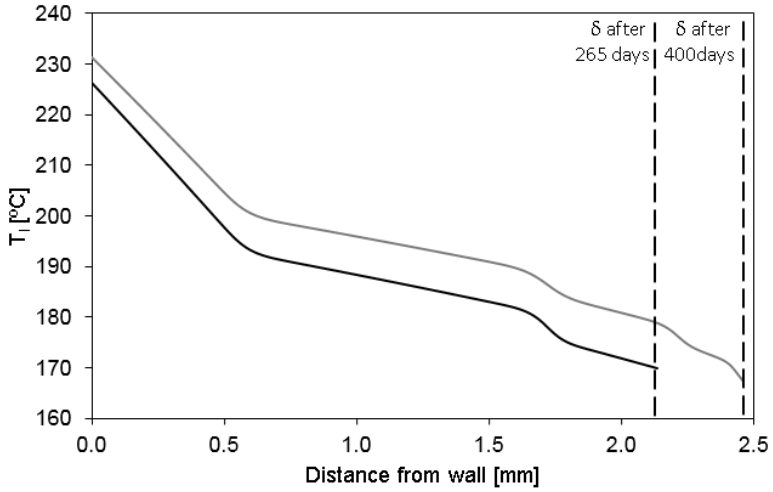

(b)

Fig. 7. Radial temperature profile in the deposit, at the exit of the 2nd pass of shell B, at the end of the operation period: after 150, 180 and 235 days (a); after 265 and 400 days (b).

The temperature difference between the wall and the deposit's surface is 39ºC. The wall is at 215ºC, but the surface of the deposit exposed to the tube-side fluid is only at 176ºC. The temperature profile is linear because the deposit is uniform in composition and conductivity in this portion. During the first inorganic breakthrough episode, occurring between days 150 and 180, a significant amount of high-inorganic content, hence higher-conductive, deposit builds up on top of the older high-organic content deposit. The result is the change in trend the

temperature profile observed in Fig. 7(a), for the 180-days line. The thickness of the deposit formed between 150 and 180 days is greater than that formed in the previous period. However, most of the temperature decay still occurs in the organic portion. The temperature decay in the newly formed inorganic-rich deposit is only 10ºC. Once the fouling returns (after day 180) to the usual behaviour, a high-organic content layer is slowly added on the deposit surface. Between days 180 and 235, the deposit grows by only 0.2 mm. The overall temperature profile after 235 days (Fig. 7a) shows two changes in trend, coinciding with the beginning and end of the first acute episode. The temperature decay through the newly formed, thin, low-conductive layer is 8ºC, of similar magnitude to that observed in the much thicker inorganic-rich portion. Overall, the occurrence of a 30-day acute inorganic breakthrough period results in the formation of a "sandwich" structure, with two low-conductive layers at the extremes which provide an insulation effect, and a high-inorganic thick portion in the middle which, in comparison, offers little resistance to heat transfer.

Fig. 7(b) shows the equivalent temperature profiles at the end of the second episode (265 days) and at the end of the operation period (400 days). Changes in trend, similar to the discussed above, are observed at the beginning and end of each acute episode. It is concluded that the deposition history and resulting spatial composition profiles have a marked impact on heat transfer. These time-varying characteristics, together with the corresponding deposit thickness, eventually determine the entire thermal and hydraulic performance of the heat exchanger, which is discussed in the next section.

3.2. Impact on Thermal and Hydraulic Performance

The ability to identify fouling events such as inorganic breakthrough is a desired feature in monitoring systems. This section explores how the insights developed earlier affect variables

that can be measured outside the heat exchanger. These are temperatures, flowrates and (less frequently) pressure drops.

Traditional fouling monitors use the fouling thermal resistance, calculated from temperature and flowrate measurements, to monitor fouling build-up. The overall fouling resistance corresponding to the simulation in the previous section is shown in Fig. 8(a).

The time profile shows an overall falling-rate behavior. The first acute episode is reflected as a slight increase in the slope of the R_f profile. The second and third acute episodes are barely noticeable. During these acute periods the deposit thickness builds-up quickly. However, the deposit formed is characterized by a higher conductivity, which partly compensates for the fast build-up from the thermal point of view. Clearly, R_f is not a suitable indicator to detect inorganics breakthrough.

The impact of the same deposition history on tube-side pressure drop is shown in Fig. 8(b). The acute inorganic deposition periods are clearly evidenced as sudden increases in pressure drop. This confirms quantitatively that the availability of these measurements is indeed essential to the detection of such changes in fouling behavior. The results motivate the implementation of pressure drop measurements, supporting the indications of other researchers and engineers in the past (e.g. ref.[9,10,12,13]). Recent examples of the use of field pressure drop measurements in fouling studies can be found in references[31,37,38].

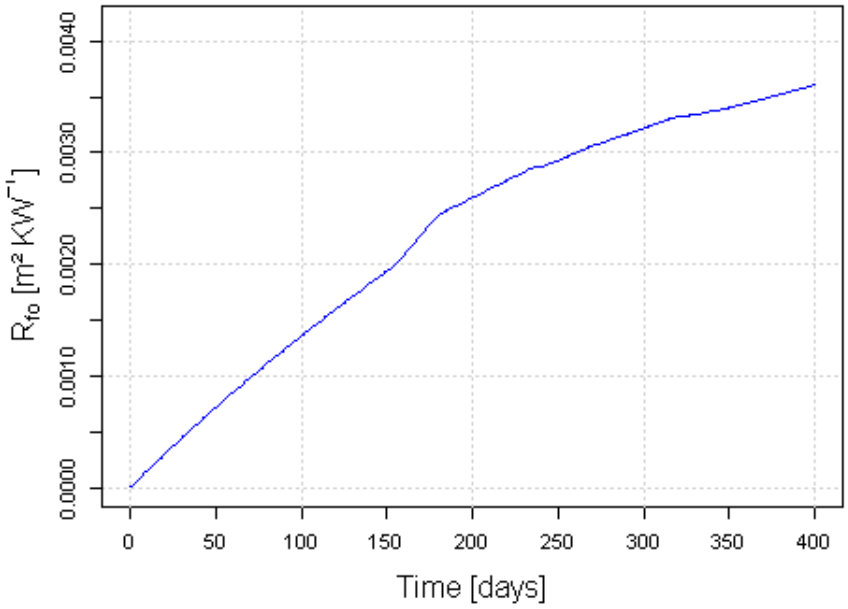

(a)

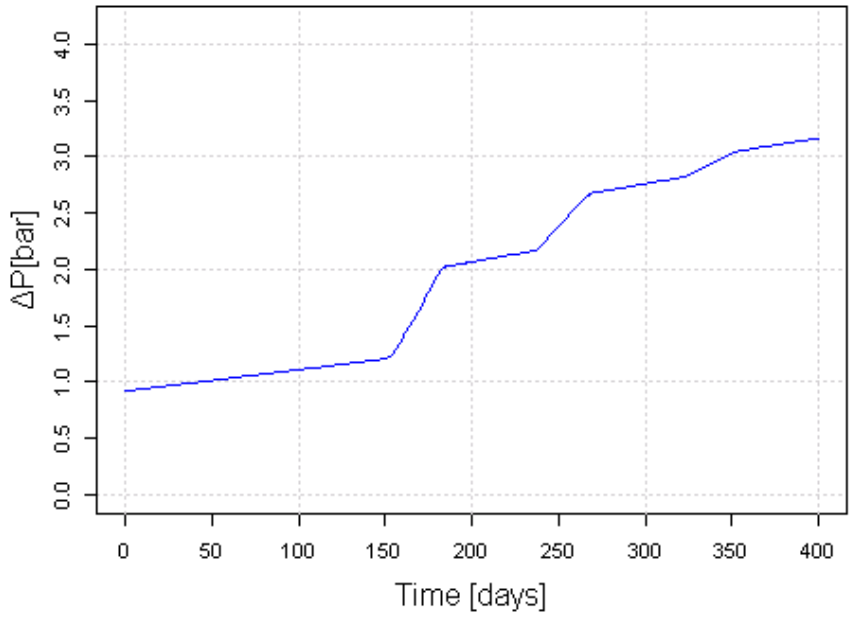

(b)

Fig. 8. Average fouling thermal resistance (a) and tube-side pressure drop (b) over 400 days of operation with intermittent inorganic breakthrough episodes.

3.3. Detection of Inorganic Breakthrough

The end question addressed in this paper is whether inorganic breakthrough can be detected based on online monitoring of measurable process conditions. As discussed earlier, the model

used here was fitted to plant data by decoupling the underlying organic fouling behavior and the inorganic deposition peaks. The predictive model resulting from that work can be used to provide a baseline for future organic-dominated fouling, which is the expected usual behavior. By comparing measured stream conditions to that baseline, it should be possible to detect changes in fouling behavior due to, for example, inorganic breakthrough.

In the following, the thermo-hydraulic response of the system with inorganic breakthrough episodes (discussed in previous sections) is compared to the expected baseline, i.e. the predicted behavior without them. The former simulates a scenario where the heat exchanger is monitored by measuring temperatures, flowrates and pressure drops. The latter represents the baseline against which the measurements are compared to. In order to make the example more realistic, Gaussian noise was added to the "monitored" signals, that is, the R_f and pressure drop profiles in Fig. 8, to simulate the measurement error. The magnitude of the added Gaussian noise and the uncertainty in the baseline prediction are based on the authors' extensive experience with plant data in industrial case studies.

Fig 9(a) shows the predicted baseline for R_f (thick line – referred to as *thermal predicted* line) and the simulated R_f under inorganic breakthrough episodes (thin line – referred to as *thermal monitored* line). The trend of the two lines is initially the same, with the monitored line fluctuating around the smooth predicted line within a measurement error calculated from the plant data of approx. 15% for R_f. During the first acute episode, the monitored line deviates almost imperceptibly towards higher R_f values. This deviation is within the measurement error and cannot be considered significant. After that, there is a change in trend of the thermal monitored line towards lower values of R_f. Only near the end of the period the deviation from the expected line is statistically larger than the error (i.e. deviation beyond the green area), however on this reading alone it would be interpreted as "good" (less fouling than expected). Consequently, monitoring based on thermal effects would not only have been ineffective in

detecting inorganic breakthrough, but also misleading in the interpretation of the actual situation. The monitored fouling resistance seems to indicate that deposition reached a plateau, with less fouling than expected, when deposition rate and tube blockage are in reality significantly greater than the predicted one.

Fig. 9(b) shows the equivalent graph to Fig. 9(a) for the tube-side pressure drop, with the *hydraulic predicted* and *hydraulic monitored* lines. In this case, the measurement error for ΔP is ± 0.2 bar. An inorganic breakthrough is clearly and rapidly captured as a deviation from the predicted hydraulic baseline during the first acute episode. The deviation shows as a sustained, constant offset after about 180 days. Fig. 10 zooms in on the period in Fig. 9(b) around the first acute episode. The deviation from the predicted baseline due to acute inorganic deposition starts on day 150. However, it is not significant until day 170, when the monitored line leaves the green area permanently. The deviation offset (Fig. 9b) increases to a new constant value after approximately day 250 and again (to a much lesser extent), around day 350, reflecting the second and third acute episodes. A similar statistical analysis can reveal when these further deviations start to become significant. The fast accumulation of material due to inorganic breakthrough could be detected by monitoring the hydraulic performance of the heat exchanger.

It is concluded that the measurement of pressure drops, in conjunction with reliable model predictions of the expected baseline, obtained using advanced thermo-hydraulic models that capture deposit composition effects, can help in the early detection of inorganics deposition.

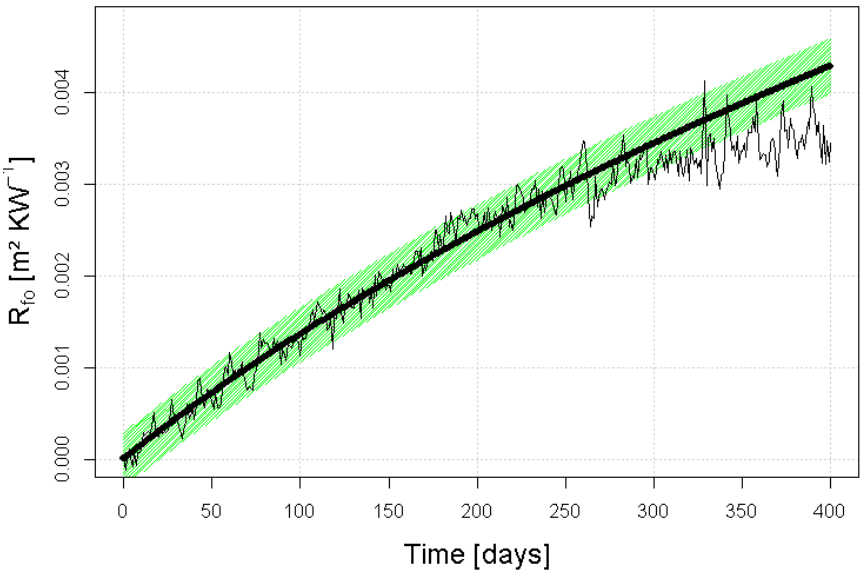

(a)

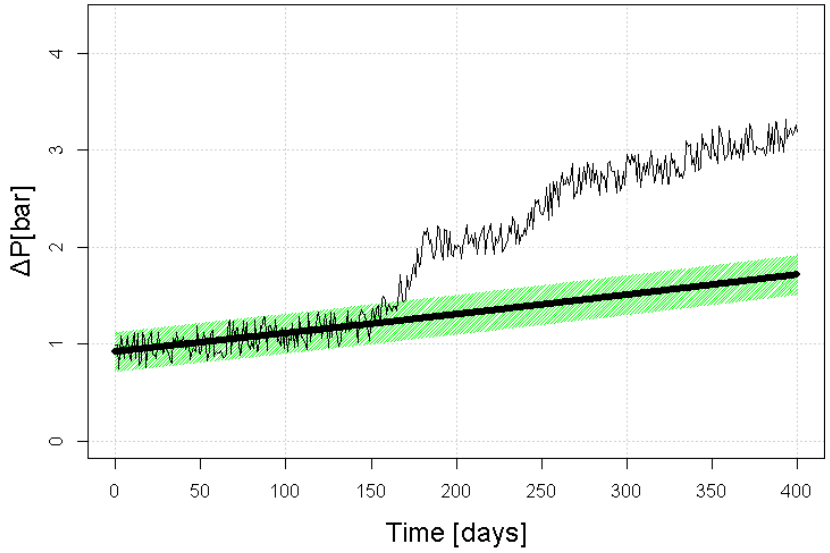

(b)

Fig. 9. Average fouling thermal resistance (a) and tube-side pressure drop (b) for expected baseline behavior (thick line; called predicted line) and scenario with intermittent inorganic breakthrough episodes (thin line; called monitored line). The green band indicates the uncertainty of the baseline prediction.

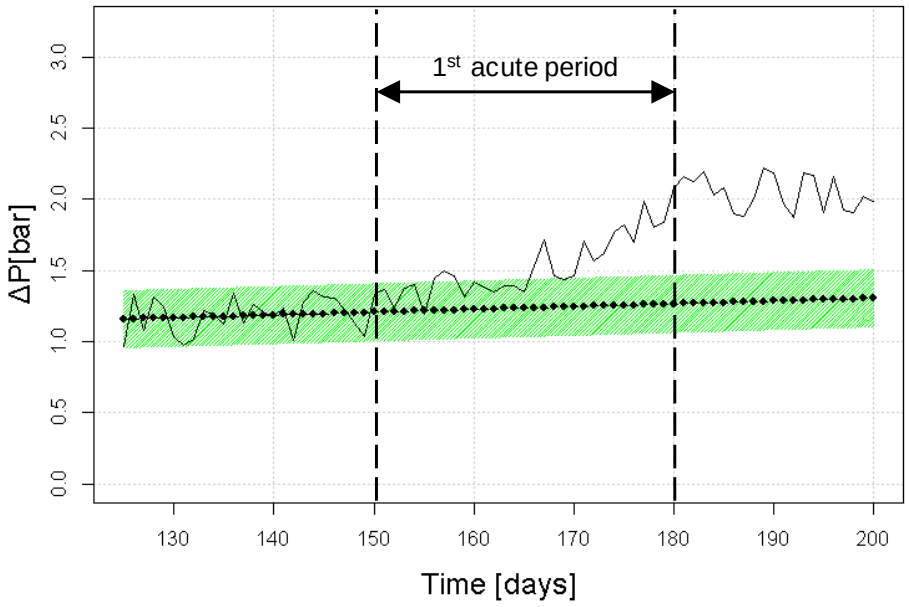

Fig. 10. Expanded version of Fig. 9(b) around the time window of the first acute episode.

3.4. Deposition Model Set-up and Validation

The deposition model set-up used in this paper was validated against industrial plant data for a heat exchanger undergoing mixed organic-inorganic deposition due to deficient desalting performance. First, the deposit local thermal conductivity was obtained from plant data, translated into composition by applying appropriate conductivity mixing models, and compared to experimental analysis[31]. The best agreement was obtained for a Co-continuous conductivity mixing model (Eq. 3, originally introduced by Wang *et al.*[35], which estimated an average inorganic content of 58_{wt}%. This result was in excellent agreement with the experimental characterization of the deposit, which gave an average inorganic content of 52_{wt}%.

Second, the presence of inorganics and their impact on the deposit conductivity was necessary to explain the impact of fouling on both pressure drop and thermal performance[37]. The proportionality ratio p_{inorg} was obtained from plant data at each time and used to decouple inorganic and organic deposition, allowing the fitting of the parameters in the threshold

correlation. The tube-side pressure drops and outlet temperatures were fitted within the uncertainty of the measurements. The result is a predictive model for the usual organic fouling behavior to be used to detect changes in trend due to inorganic deposition. A preliminary paper on experimental verification was presented at the HEFAT 2015 conference[27] and details will be presented in future publications[37].

4. DISCUSSION

The modelling approach used in this work has been shown to efficiently track the deposition history over an industrially relevant simulated time horizon, capturing multiple changes in fouling behavior and the impact of complex deposit layers on overall exchanger performance.

The composition, conductivity and temperature profiles (Fig. 5-7), reflect changes in composition at the deposit surface (i.e. changes in deposition rate), and the ability to capture such effects at their impact on the overall thermal and hydraulic performance. The history tracking capabilities of the deposit model used in this work cannot be achieved with more simplified models. Its application to industrial relevant examples was demonstrated, and an initial validation made by comparing the predicted composition to the average inorganic content of collected deposits, as discussed in the Model Description section. A further validation of the approach would require the comparison of simulated composition profile (such as that in Fig. 5) to a measured composition profile from intact deposit samples.

From the practical point of view, the case study in this paper shows that hydraulic measurements are required to *detect* acute deposition. However, the *diagnosis* of the acute deposition as being due to inorganics requires the simultaneous consideration both thermal and hydraulic aspects. While acute inorganic fouling is characterized by high hydraulic impact and

moderate-low thermal impact, with acute fouling of organic nature both thermal and hydraulic performance are severely affected. A detailed discussion is provided by Diaz-Bejarano *et al*.[28].

The combined used of plant measurements and predictive models for the expected behavior (baseline) helps to early and unambiguously detect and diagnose changes in fouling behavior. The example previously discussed here show that it was possible to detect and diagnose the acute inorganics breakthrough within a few days of the first acute episode starting. This would allow rapid remedial actions.

The time required to detect a statistically significant deviation in fouling behavior depends on the accuracy of the measurements, the accuracy and reliability of the model predictions and the timing of the event itself. As discussed by Diaz-Bejarano *et al*.[28], acute fouling episodes occurring at the early stages (with an almost clean exchanger) are more easily detected with thermal measurements, whilst similar episodes occurring at the late stages (after significant previous fouling build-up) are more easily detected with hydraulic measurements. In any case, the combination of both is necessary to diagnose the nature of the deposit.

5. CONCLUSIONS

A deposit model, capable of capturing simultaneously the deposition of both organic and inorganic species, was used to track deposition history in a refinery shell-and-tube heat exchanger undergoing intermittent acute fouling due to inorganics breakthrough from the desalter. The conclusions of the case study are:

1. Intermittent acute deposition of inorganic results in a deposit with complex layered structure.
2. The amount of deposit build-up determines the hydraulic performance of the exchanger, whilst the nature of the deposit (characterized by a radial composition profile) determines its conductivity profile and, ultimately, the thermal performance of the exchanger.

3. The above effects can only be captured by using a deposit model with the ability to track deposition history.
4. Acute inorganic deposition may be detected by measuring pressure drops, but could pass undetected by traditional R_f monitors.
5. A combination of thermo-hydraulic measurements and reliable predictive models that can track deposit history can be used to detect and diagnose acute inorganic deposition episodes in a short time (days or weeks, depending on the quality of the measurements and timing of the events).
6. This enables to quickly alert plant operators of unexpected events such as breakthrough of inorganics at an early stage, and help in planning corrective actions.
7. Further validation may be done by comparing the estimated results from the approach against experimental characterization of deposits collected during shutdown.

NOMENCLATURE

C_p Specific heat capacity, J/kg K

$c_{l,i}$ Concentration of component i in the layer, kg/m^3

E_f Deposition activation energy, J/mol

n Mass flux, kg/m^2 s

N Number of components in the layer

NR Number of reactions

p_{inorg} Inorganic-to-organic deposition rate proportionality ratio, dimensionless

Pr Prandtl number, dimensionless

R_i Inner Radius, m

R_f Fouling resistance, m^{2}K/W

r_j Rate of reaction j, kg/ m^3 s

$\tilde{r}$ Dimensionless radial coordinate, dimensionless

Re Reynolds number, dimensionless

t Time, s

T Temperature, K

x Volume fraction, m^3/ m^3

z Axial coordinate, m

α' Deposition constant, kg/m^2s

γ' Removal constant, kg/m^2sPa

δ Deposit thickness, m

$\dot{\delta}$ Rate of change of fouling layer thickness, m/ s

ΔP Pressure drop, bar

λ Thermal conductivity, W/mK

ρ Density, kg/m^2

ν_{ij} Stoichiometric coefficient for component i in reaction j

τ_w Wall shear stress, Pa

Ω Spatial domain

Subscript

i Component number

in Inlet

inorg Inorganic

j Reaction number

l Layer

n Pass number

o Outer tube area

org Organic

s Shell-side flow

t Tube-side flow

w Tube wall

REFERENCES

1. Macchietto S, Hewitt GF, Coletti F, et al. Fouling in Crude Oil Preheat Trains: A Systematic Solution to an Old Problem. *Heat Transf Eng*. 2011;32(3-4):197-215.
2. Ebert WA, Panchal CB. Analysis of Exxon crude-oil-slip stream coking data. In: Panchal CB, ed. *Fouling Mitigation of Industrial Heat-Exchange Equipment*. San Luis Obispo, California (USA): Begell House; 1995:451-460.
3. Nasr MRJ, Givi MM. Modeling of crude oil fouling in preheat exchangers of refinery distillation units. *Appl Therm Eng*. 2006;26(14-15):1572-1577.
4. Deshannavar UB, Rafeen MS, Ramasamy M, Subbarao D. Crude oil fouling a review. *J Appl Sci*. 2010;10(24):3167-3174.
5. Coletti F, Crittenden BD, Haslam AJ, et al. Modelling of Fouling from Molecular to Plant Scale. In: Coletti F, Hewitt GF, eds. *Crude Oil Fouling: Deposit Characterization, Measurements, and Modeling*. Boston: Gulf Professional Publishing; 2014.
6. Wang Y, Yuan Z, Liang Y, Xie Y, Chen X, Li X. A review of experimental measurement and prediction models of crude oil fouling rate in crude refinery preheat trains. *Asia-Pacific J Chem Eng*. 2015;10:607-625.
7. Wilson, D.I., Ishiyama EM, Polley GT. Twenty Years of Ebert and Panchal—What Next? *Heat Transf Eng*. 2017;38(7-8):669-680.
8. Diaz-Bejarano E, Coletti F, Macchietto S. A new dynamic model of crude oil fouling deposits and its application to the simulation of fouling-cleaning cycles. *AIChE J*. 2016;62(1):90-107.
9. Chenoweth JM. General Design of Heat Exchangers for Fouling Conditions. In: Melo

LF, Bott TR, Bernardo CA, eds. *Fouling Science and Technology*. Vol 145. NATO ASI Series. Springer Netherlands; 1988:477-494. doi:10.1007/978-94-009-2813-8_32.

10. Yeap BL, Wilson DI, Polley GT, Pugh SJ. Mitigation of crude oil refinery heat exchanger fouling through retrofits based on thermo-hydraulic fouling models. *Chem Eng Res Des*. 2004;82(1):53-71.
11. Ishiyama EM, Paterson WR, Wilson DI. The Effect of Fouling on Heat Transfer, Pressure Drop, and Throughput in Refinery Preheat Trains: Optimization of Cleaning Schedules. *Heat Transf Eng*. 2009;30(10-11):805-814.
12. Polley GT, Morales-Fuentes A, Wilson DI. Simultaneous Consideration of Flow and Thermal Effects of Fouling in Crude Oil Preheat Trains Simultaneous Consideration of Flow and Thermal Effects of Fouling. *Heat Transf Eng*. 2009;30(10-11):815-821. doi:10.1080/01457630902751494.
13. Coletti F, Macchietto S, Polley GT. Effects of fouling on performance of retrofitted heat exchanger networks: A thermo-hydraulic based analysis. *Comput Chem Eng*. 2011;35(5):907-917.
14. Crittenden BD, Kolaczkowski ST, Downey IL. Fouling of Crude Oil Preheat Exchangers. *Trans IChemE, Part A, Chem Eng Res Des*. 1992;70:547-557.
15. Srinivasan M, Watkinson AP. Fouling of Some Canadian Crude Oils. *Heat Transf Eng*. 2005;26(1):7-14.
16. Bennett CA, Kistler RS, Nangia K, Al-Ghawas W, Al-Hajji N, Al-Jemaz A. Observation of an Isokinetic Temperature and Compensation Effect for High-Temperature Crude Oil Fouling. *Heat Transf Eng*. 2009;30(10-11):794-804.
17. Venditti S, Berrueco C, Alvarez P, et al. Developing Characterisation Methods for Foulants Deposited in Refinery Heat Exchangers. In: Müller-Steinhagen H, Malayeri MR, Watkinson AP, eds. *International Conference on Heat Exchanger Fouling and*

Cleaning VIII. Schladming, Austria; 2009:44-51.

18. Fan Z, Rahimi P, McGee R, Wen Q, Alem T. Investigation of fouling mechanisms of a light crude oil using an alcor hot liquid process simulator. *Energy and Fuels*. 2010;24(11):6110-6118. doi:10.1021/ef101097c.
19. Young A, Venditti S, Berrueco C, et al. Characterization of Crude Oils and Their Fouling Deposits Using a Batch Stirred Cell System. *Heat Transf Eng*. 2011;32(3-4):216-227.
20. Joshi HM. Analysis of Field Fouling Deposits from Crude Heat Exchangers. In: Coletti F, Hewitt GF, eds. *Crude Oil Fouling: Deposit Characterization, Measurements, and Modeling*. Boston: Gulf Professional Publishing; 2014.
21. Mozdianfard MR, Behranvand E. A field study of fouling in CDU preheaters at Esfahan refinery. *Appl Therm Eng*. 2013;50(1):908-917.
22. Mozdianfard MR, Behranvand E. Fouling at post desalter and preflash drum heat exchangers of CDU preheat train. *Appl Therm Eng*. 2015;89:783-794.
23. Müller-Steinhagen H, Malayeri MR, Watkinson AP. Heat Exchanger Fouling: Mitigation and Cleaning Strategies. *Heat Transf Eng*. 2011;32(3-4):189-196.
24. Bott TR. *Fouling of Heat Exchangers*. 1st ed. Amsterdam: Elsevier Science; 1995.
25. Shackelford JF, Alexander W. *CRC Materials Science and Engineering Handbook*. 3rd ed. London: CRC press; 2000.
26. Wang W, Watkinson AP. Iron Sulphide and coke fouling from sour oils: review and initial experiments. In: Malayeri MR, Müller-Steinhagen H, Watkinson AP, eds. *Int. Conf. on Heat Exchanger Fouling and Cleaning 2011*. Vol 2011. Crete Island, Greece; 2011:23-30.
27. Diaz-Bejarano E, Coletti F, Macchietto S. Impact of Crude Oil Fouling Composition on the Thermo-Hydraulic Performance of Refinery Heat Exchangers. In: *11th International*

Conference on Heat Transfer, Fluid Mechanics and Thermodynamics. Kruger National Park, South Africa; 2015.

28. Diaz-Bejarano E, Coletti F, Macchietto S. Impact of Complex Layering Structures of Organic and Inorganic Foulants on the Thermohydraulic Performance of a Single Heat Exchanger Tube: A Simulation Study. *Ind Eng Chem Res*. 2016;55(40):10718-10734. doi:10.1021/acs.iecr.6b02330.
29. Hexxcell Ltd. Hexxcell Studio. http://www.hexxcell.com. Published 2017.
30. Coletti F, Macchietto S. A Dynamic, Distributed Model of Shell-and-Tube Heat Exchangers Undergoing Crude Oil Fouling. *Ind Eng Chem Res*. 2011;50(8):4515-4533.
31. Diaz-Bejarano E, Behranvand E, Coletti F, Mozdianfard MR, Macchietto S. Organic and Inorganic Fouling in Heat Exchangers – Industrial Case Study: Analysis of Fouling State. *Appl Energy*. 2017;206:1250-1266.
32. Holman JP. *Heat Transfer*. 8th ed. London: McGraw-Hill; 2001.
33. Saunders EAD. *Heat Exchangers: Selection, Design, and Construction*. Longman, Harlow; 1988.
34. Taborek J. Shell-and-tube heat exchangers: single phase flow. In: Hewitt GF, ed. *Heat Exchanger Design Handbook*. New York: Begell House; 2002.
35. Wang J, Carson JK, North MF, Cleland DJ. A new structural model of effective thermal conductivity for heterogeneous materials with co-continuous phases. *Int J Heat Mass Transf*. 2008;51(9-10):2389-2397.
36. Panchal CB, Kuru WC, Liao CF, Ebert WA, Palen JW. Threshold conditions for crude oil fouling. In: Bott TR, Melo LF, Panchal CB, Somerscales EFC, eds. *Understanding Heat Exchanger Fouling and Its Mitigation*. NY: Begell House; 1999:273-279.
37. Diaz-Bejarano E, Behranvand E, Coletti F, Mozdianfard MR, Macchietto S. Organic and Inorganic Fouling in Heat Exchangers – Industrial Case Study: Analysis of Fouling

Rate. *Submitt Publ*. 2018.

38. Chunangad KS, Chang RY, Casebolt RP. Evaluation and Prediction of the Thermal and Hydraulic Impact of Crude Oil Fouling on Exchanger Performance using Pressure Measurements. In: *Heat Exchanger Fouling and Cleaning - 2017*. Aranjuez (Madrid), Spain; 2017:1-4.